BRAIN
ORIGINAL ARTICLE

# Molecular trans-dural efflux to skull bone marrow in humans with CSF disorders

**Geir Ringstad[1] and Per Kristian Eide[2,3]**

Dural sinuses were recently identified as a hub for peripheral immune surveillance of brain-derived antigens cleared through CSF. However, animal studies have also indicated that substances and cells may enter the intracranial compartment directly from bone marrow.

We used MRI and a CSF tracer to investigate *in vivo* whether intracranial molecules can move via dura to skull bone marrow in patients with suspicion of CSF disorders. Tracer enrichment in CSF, dural regions and within skull bone marrow was assessed up to 48 h after intrathecal administration of gadobutrol (0.5 ml, 1 mmol/ml) in 53 patients. In participants diagnosed with disease, tracer enrichment within diploe of skull bone marrow was demonstrated nearby the parasagittal dura, nearby extensions of parasagittal dura into diploe, and in diploe of skull bone remote from the dura extensions.

This crossing of meningeal and skull barriers suggests that bone marrow may contribute in brain immune surveillance also in humans.

1 Department of Radiology, Oslo University Hospital-Rikshospitalet, Pb 4950 Nydalen, N-0424 Oslo, Norway
2 Department of Neurosurgery, Oslo University Hospital-Rikshospitalet, Pb 4950 Nydalen, N-0424 Oslo, Norway
3 Institute of Clinical Medicine, Faculty of Medicine, University of Oslo, PB 1072 Blindern, N-0316 Oslo, Norway

Correspondence to: Per Kristian Eide, MD, PhD
Department of Neurosurgery
Oslo University Hospital—Rikshospitalet
Pb 4950 Nydalen, N-0424 Oslo, Norway
E-mail: p.k.eide@medisin.uio.no

Keywords: bone marrow; immune system; dural lymphatic vessels; parasagittal dura

Abbreviations: BB = black blood; De = dural extension; PSD = parasagittal dura; PSDe = parasagittal dura extensions

## Introduction

Compared to other organs, the CNS has been considered immune-privileged as its vulnerable cells are protected from entry of leukocytes into parenchyma by the intact blood–brain barrier.[1] Yet, research breakthroughs made in recent years have demonstrated that cross-talk at neuroimmune interfaces can occur outside the CNS surface. The dura mater of the skull and spinal canal harbours true lymphatic vessels that were shown to drain substances/brain-specific solutes directly from CSF.[2–4] In particular, human CSF has been shown to drain directly into dura of the parasagittal region.[5] Both lymphatic vessels and blood vessels within the dura lack tight junctions,[6] potentially allowing for two-way molecular passage. Recently, a rodent study reported that CNS immune surveillance occurs in the perisinus region by presentation of brain-derived antigens to T cells before local lymphatic drainage, enabled by venous sinus endothelial and stromal cells forming a sinus stromal niche.[7]

Received May 24, 2021. Revised September 24, 2021. Accepted October 5, 2021. Advance access publication November 25, 2021

From rodent skull bone marrow,[8] myeloid cells can directly cross the inner skull cortex to dura through microscopic channels. Skull bone permeability was also confirmed by diffusional penetration of <40 000 molecular weight compounds from bone marrow over to meninges.[9] In addition to dendritic cells, neutrophils may act as antigen-presenting cells within dura and regulate T-cell function.[10] Furthermore, immune cells can be released directly from dura into CSF and take part in acute neuroinflammation,[11] even in remote areas of the CNS.[12] Transport from dura to the subarachnoid compartment across the arachnoid barrier, which has a continuous system of tight junctions, is likely to be regulated and to occur in specialized regions, however, a detailed analysis of region-specific differences remains to be performed.[13]

Evidence for immunological cross-talk between brain and bone marrow in humans is scarce. One study depicted microscopic channels of the inner skull cortex bone, rendering for the existence of such a direct route,[11] and a PET study detected inflammation in bone marrow directly adjacent to brain regions of cortical spreading depression in migraine patients.[14] It remains, however, to be demonstrated any functional cranial communication between CSF and skull bone marrow in human subjects. As CSF can potentially carry nutrients and waste solutes to and from the entire brain,[15,16] the implications of a direct route for communication between bone marrow and CSF could shed new light on CSF molecular drainage and neuro-inflammatory brain disorders.

In this study, our aim was therefore to explore the hypothesis that CSF drains via dura to intradiploic bone marrow of the skull vertex adjacent- and remote to parasagittal dura (PSD). For this, we used the hydrophilic MRI contrast agent gadobutrol as CSF tracer, which was injected intrathecally in patients under clinical work-up of various CSF disorders. As previously shown,[5] MRI can readily identify dural tissue, and $T_1$ black blood (BB) imaging can sensitively detect tracer enrichment, which was assessed in vertex regions of CSF, dura and skull at consecutive imaging for up to 48 h.

## Materials and methods

This study was approved by the following: The Institutional Review Board (2015/1868), Regional Ethics Committee (2015/96) and the National Medicines Agency (15/04932–7), and registered in Oslo University Hospital Research Registry (ePhorte 2015/1868). Inclusion was after written and oral informed consent.

### Experimental design

We followed a prospective and observational study protocol. It was not relevant with randomization of patients or a priori sample size calculation.

### Patients

We included consecutive individuals referred to the Department of Neurosurgery, Oslo University Hospital—Rikshospitalet, Oslo, Norway, for various CSF circulation disorders (Table 1). Individuals with a history of hypersensitivity reactions to contrast media agents, severe allergy reactions in general, evidence of renal dysfunction (i.e. normal glomerular filtration rate, GFR), age <18 or >80 years were not included, neither were individuals who were pregnant or breastfeeding.

### MRI protocol

Scans were obtained in a 3 T MRI unit (Philips Ingenia®) with a 32-channel head coil.

Details for whole-brain 3D $T_2$-fluid attenuated inversion recovery (FLAIR): repetition time (TR)/echo time (TE)/inversion time (TI) = 4800/311/1650 ms, echo train length = 167, flip angle = 90°, two averages, 1 × 1 × 1 mm voxel size (isotropic) and acquisition time = 5 min 41 s.

Details for whole-brain 3D $T_1$-BB: TR/TE = 700/35 ms, echo train length = 55, flip angle = 80°, two averages, 1 × 1 × 1 mm voxel size (isotropic) and acquisition time 4 min 54 s.

Details for whole-brain 3D $T_1$-gradient echo: TR = shortest (typically 5.1 ms); echo time = shortest (typically 2.3 ms); echo train length = 232; flip angle = 8°, one average, 1 × 1 × 1 mm voxel size and acquisition time 6 min 29 s.

The MRI acquisitions were repeated at 3, 6, 24 and 48 h after intrathecal injection of 0.5 ml gadobutrol (1 mmol/ml) (Gadovist®, Bayer AB). Intrathecal injection was performed by an experienced interventional neuroradiologist under fluoroscopic guidance at the lower lumbar level. Correct needle (22G) position within the lumbar subarachnoid space was confirmed by backflow of CSF. Patients were instructed to remain in the supine position with a head pillow until the last imaging procedure at day 1 (at about 4 p.m.), thereafter free movement was allowed.

The $T_2$-FLAIR acquisitions suppress free (unbound) CSF within the ventricular compartment and subarachnoid space.[17] $T_1$-BB images are tuned to darken the contents of blood vessels, even when containing a contrast agent.[18] Thereby, the $T_1$-BB signal is nulled in areas with moving protons, e.g. arteries and veins. Over the high brain convexities little motions within the CSF makes the signal not black (nulled) as in the blood vessels, which renders for a more intermediate CSF-signal. We applied $T_2$-FLAIR to identify the regions of interest and the $T_1$-BB to semi-quantify change in normalized signal unit ratio over time; a comparison of imaging using $T_2$-FLAIR and $T_1$-BB is shown in Supplementary Fig. 1.

### Image analysis

Sagittal $T_2$-fluid FLAIR and $T_1$-BB scans from all time points were reformatted into coronal and axial 1-mm slices perpendicular and parallel to the plane defined by a line between the anterior and posterior commissures (AC-PC plane), respectively. Identically positioned coronal slices were applied to identify PSD with tissue signal remaining unsuppressed (intermediate or high signal) at both $T_2$-FLAIR and $T_1$-BB. All regions of interest were manually placed in the images by a radiologist with 15 years of experience in neuroradiology (G.R.), adapting each region of interest for robust placement within the borders of each area of interest to avoid partial averaging effects from neighbouring structures. All regions of interest were placed blinded to the signal and in the same locations throughout all time points in each patient. Tracer enrichment was assessed as change in $T_1$-BB signal units, and was normalized against reference regions of interest placed within the vitreous body of the ocular bulbs, respectively, using the average signal intensity, to correct for baseline shifts of image greyscale between time points.

### 3D illustrations

For 3D representations, FLAIR-MRI was used for segmentation of PSD and skull, 3D $T_1$-gradient echo was used for segmentation of the brain surface and $T_1$-BB subtraction (24 h post-contrast minus pre-contrast) was used for visualization of tracer enhancement in CSF and PSD. Segmentation and coregistration were done in 3D Slicer v.4 and SPM 12 (both open source software) (Fig. 1 and Supplementary Fig. 2).

### Locations with tracer enrichment

We examined tracer enrichment within three main regions of interest, namely CSF, PSD and De into skull bone marrow, either

**Table 1 Information about the patient material and the different types of dural structures visualized by MRI $T_2$-FLAIR**

| Patient material | | Categories of dural structures | | | |
|---|---|---|---|---|---|
| | | PSD (no PSDe or De) | PSD + PSDe | PSD + De | PSD + PSDe + De |
| *n* | 53 | 21 (40%) | 20 (38%) | 5 (9%) | 7 (13%) |
| Age (years) | 43.5 ± 15.0 | 39.2 ± 13.8 | 44.1 ± 12.7 | 33.3 ± 6.2 | 62.4 ± 14.4 |
| Gender (female/male) | 39/14 | 16/5 | 14/6 | 5/0 | 4/3 |
| Body mass index (kg/m$^2$) | 27.9 ± 5.2 | 28.6 ± 5.7 | 28.2 ± 4.3 | 27.7 ± 7.8 | 25.5 ± 4.4 |
| Diagnosis | | | | | |
| Reference subjects | 15 (28%) | 6 (29%) | 6 (30%) | 2 (40%) | 1 (14%) |
| Idiopathic normal pressure hydrocephalus | 3 (6%) | 1 (5%) | 1 (5%) | 0 | 1 (14%) |
| Spontaneous intracranial hypotension | 7 (13%) | 2 (10%) | 3 (15%) | 1 (20%) | 1 (14%) |
| Arachnoid cyst | 9 (17%) | 1 (5%) | 5 (25%) | 0 | 3 (43%) |
| Pineal cyst | 3 (6%) | 1 (5%) | 2 (10%) | 0 | 0 |
| Idiopathic intracranial hypertension | 11 (21%) | 6 (29%) | 3 (15%) | 2 (40%) | 0 |
| Communicating hydrocephalus | 3 (6%) | 2 (10%) | 0 | 0 | 1 (14%) |
| Dementia | 2 (4%) | 2 (10%) | 0 | 0 | 0 |

Data are given as mean ± SE.

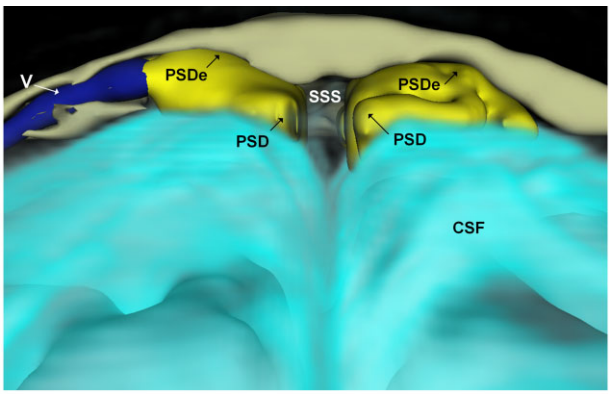


**Figure 1 3D representation (coronal plane) illustrating dural extensions from PSD into the intradiploic bone marrow space at skull vertex.** The PSD (yellow) directly overlies the CSF within the subarachnoid space (turquoise). An intradiploic vein (V; dark blue) traverses within the skull bone marrow (beige) adjacent to the PSD. It can be noted how the PSD extends into the intradiploic bone marrow space (PSDe). The different colours of CSF and PSD/PSDe reflect different tracer enrichments. Image: Tomas Sakinis, MD.

directly adjacent to each of PSD (parasagittal dura extensions, PSDe) and De, and in skull bone marrow. Supplementary Fig. 3 shows placement of regions of interest for assessment of $T_1$-BB signal increase.

### Subarachnoid CSF spaces

The tracer enrichment within CSF of subarachnoid space was examined both in subarachnoid spaces nearby PSD and nearby dural extensions into diploic bone marrow in distance from PSD.

### Parasagittal dura and dura extensions into diploe of skull bone marrow

Tracer enrichment was determined within dural tissue that was continuous with PSD at FLAIR extending through the inner table to diploic area of skull bone marrow (referred to as PSDe). In the case of several separate extensions, the most prominent was selected for region of interest measurement. We also determined tracer enrichment in dural extensions (De) into diploe of skull bone marrow in the distance from PSD. These structures include tissue with FLAIR-signal similar to PSD, but not continuous with PSD, extending through inner table to diploic compartment. In those cases with several dural extensions, the most prominent was selected for region of interest measurement.

### Skull bone marrow

We examined tracer enrichment in skull bone marrow in four different locations: (i) skull bone marrow nearby PSD; (ii) skull bone marrow nearby dural extensions into diploe from PSD; (iii) skull bone marrow nearby dural extensions into diploe in distance from PSD; and (iv) skull bone marrow in distance from dura locations, which was denoted 'remote skull bone marrow'.

### Statistics

Statistical analyses were performed using the SPSS software v.25 (IBM Corporation, Armonk, NY, USA). Differences between continuous data were determined using linear mixed models with a random intercept. Correlations were determined by Pearson correlation coefficient. Statistical significance was accepted at the 0.05 level (two-tailed).

### Data availability

The data presented in this work are available on request.

## Results

### Study material

The study included 53 patients under clinical work-up for possible CSF disorders (Table 1). Fifteen individuals without any subsequent diagnose of CSF disturbance were denoted reference subjects; the remaining 38 patients were diagnosed with various intracranial pathologies (Table 1).

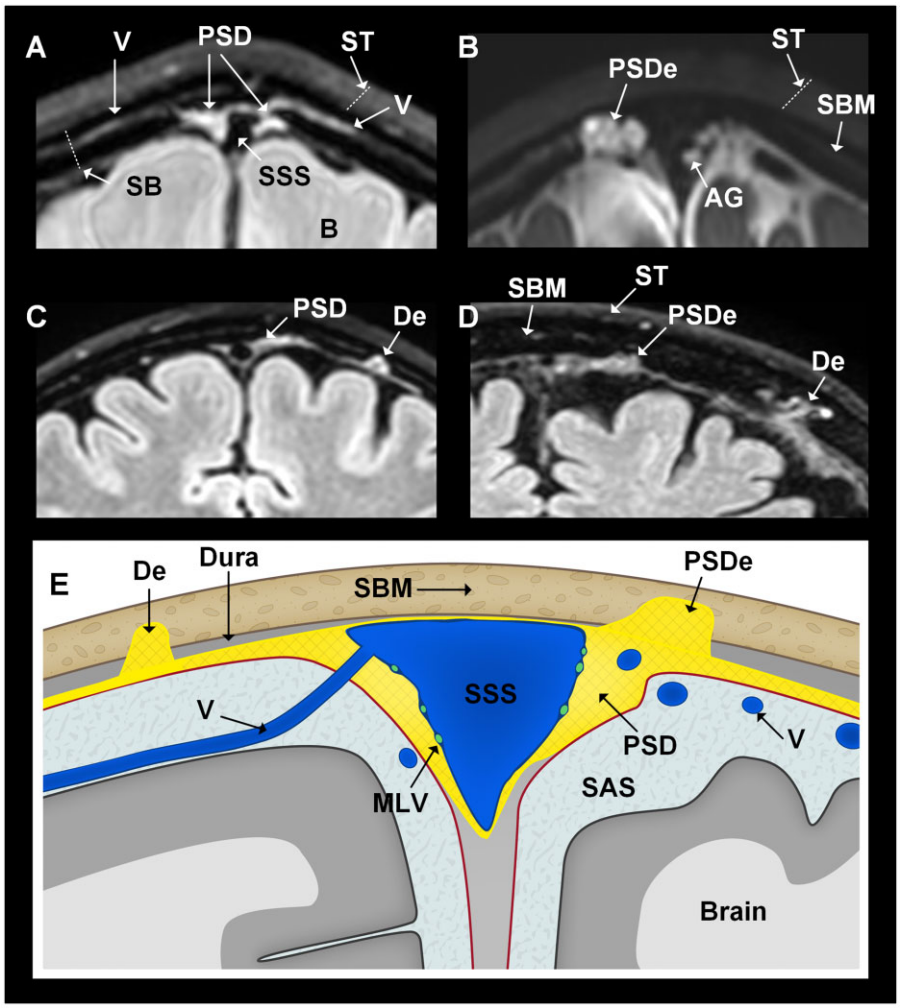


**Figure 2 Patients with dural extensions into bone marrow of skull, either directly or in distance from PSD (all coronal sections at skull vertex).** In this study, we examined three main intradural locations, namely the parasagittal dura (PSD), parasagittal dura extensions (PSDe) into dipolic area of skull bone marrow and dural extensions (De) into skull bone marrow, but not in direct continuity with PSD. Examples are retrieved from four different patients. (**A**) The PSD is a loose soft tissue matrix adjacent to the superior sagittal sinus (SSS), here visualized by $T_2$-FLAIR. (**B**) The PSDe cross the inner table into the diploe of skull, and are separated from the subarachnoid space (SAS). It is different from macroscopically visible arachnoid granulations (AG) bulging into the sinus. Here, both PSDe and AG are enriched by CSF tracer ($T_1$-BB, 24 h). (**C**) In distance from PSD, De into diploic area of skull bone marrow (SBM) may be seen ($T_2$-FLAIR). (**D**) The size and shape of parasagittal and dural extensions (PSDe, De) vary considerably ($T_2$-FLAIR). (**E**) Cartoon illustrating the examined anatomical structures beyond the superficial tissue ($T_2$-FLAIR). MLV = meningeal lymphatic vessels; ST = superficial tissue. Illustration in **E**: Øystein Horgmo, University of Oslo.

## Parasagittal dura and intradiploic extensions

Presence of PSD was confirmed at FLAIR in 53/53 (100%) study subjects (Fig. 2A), however, with variations in prominence (Supplementary Figs. 4–7). PSD crossed the inner table of the skull and extended into the intradiploic bone marrow space (PSDe) in 27/53 individuals (51%) (Fig. 2B), and dural tissue remote to PSD extended into the intradiploic space (De) in 12/53 subjects (23%; Fig. 2C and D), whereas the combination of both features occurred in 7/53 (13%) (Table 1). The anatomy of these structures varies between patients, as shown in Fig. 2A–D and Supplementary Figs 4–7. A cartoon (Fig. 2E) illustrates the anatomical structures.

## Tracer enrichment in CSF spaces

The intrathecal tracer strongly enriched CSF within the subarachnoid space (Supplementary Fig. 8). The increased normalized $T_1$-BB signal provides a semi-quantitative estimation of tracer enrichment, and was increased markedly in CSF nearby the PSD and nearby the dural extensions (De) to diploe of skull bone (Table 2 and Fig. 3).

## Tracer enrichment in different intradural locations

Figure 1 and Supplementary Fig. 2 show 3D illustrations of tracer enrichment within dural tissue extending into diploe of skull bone marrow. The change in $T_1$-BB signal units, indicative of tracer enrichment, is further illustrated in Supplementary Fig. 9. At group level, the CSF tracer enriched the PSD of 47/53 patients with peak at 24 h (Fig. 4A). In the 6/53 patients without tracer enrichment in PSD, this was accompanied with lack of enrichment in the adjacent CSF space ($n = 5$) and small size of PSD ($n = 1$), not allowing for robust measurements. Furthermore, enrichment was found in PSDe in 27/47 (57%) patients, also with a peak at 24 h (Fig. 4B). The tracer enriched De in 12/47 (26%) individuals and was still trending upwards at 48 h (Fig. 4C). In Table 2 is presented an overview of

**Table 2 Information about change in normalized $T_1$-BB signal units over time for the different regions of interest**

| | Normalized $T_1$-BB signal units | | | | | Percentage change from Pre of normalized $T_1$-BB signal units | | | |
|---|---|---|---|---|---|---|---|---|---|
| | Pre | 3 h | 6 h | 24 h | 48 h | 3 h | 6 h | 24 h | 48 h |
| **Locations in subarachnoid CSF space** | | | | | | | | | |
| Nearby PSD | 1.34 ± 0.06 | 2.25 ± 0.35$^{b}$ | 3.80 ± 0.59$^{c}$ | 5.13 ± 0.46$^{c}$ | 3.99 ± 0.30$^{c}$ | 76 ± 30$^{a}$ | 191 ± 42$^{c}$ | 298 ± 34$^{c}$ | 200 ± 23$^{c}$ |
| Nearby De | 1.32 ± 0.04 | 2.33 ± 0.81 | 3.14 ± 0.95 | 5.59 ± 0.57$^{c}$ | 5.14 ± 0.49$^{c}$ | 78 ± 61 | 140 ± 61$^{a}$ | 322 ± 36$^{c}$ | 292 ± 39$^{c}$ |
| **Locations within dura** | | | | | | | | | |
| PSD | 1.51 ± 0.06 | 2.02 ± 0.15$^{c}$ | 2.78 ± 0.24$^{c}$ | 3.49 ± 0.32$^{c}$ | 2.88 ± 0.21$^{c}$ | 38 ± 10$^{c}$ | 91 ± 14$^{c}$ | 134 ± 21$^{c}$ | 92 ± 15$^{c}$ |
| PSDe | 1.48 ± 0.06 | 2.03 ± 0.19$^{b}$ | 2.97 ± 0.37$^{c}$ | 4.02 ± 0.48$^{c}$ | 3.38 ± 0.29$^{c}$ | 41 ± 12$^{b}$ | 109 ± 23$^{c}$ | 177 ± 33$^{c}$ | 125 ± 20$^{c}$ |
| De | 1.47 ± 0.08 | 1.58 ± 0.15 | 1.95 ± 0.23$^{a}$ | 3.50 ± 0.55$^{c}$ | 3.72 ± 0.49$^{c}$ | 8 ± 9 | 31 ± 13$^{a}$ | 144 ± 37$^{c}$ | 154 ± 30$^{c}$ |
| **Locations in skull bone marrow** | | | | | | | | | |
| Skull nearby PSD | 0.27 ± 0.03 | 0.31 ± 0.03$^{a}$ | 0.30 ± 0.03$^{a}$ | 0.30 ± 0.03$^{a}$ | 0.29 ± 0.03 | 26 ± 10$^{b}$ | 24 ± 11$^{a}$ | 22 ± 6$^{b}$ | 11 ± 8 |
| Skull nearby PSDe | 0.32 ± 0.05 | 0.37 ± 0.05$^{a}$ | 0.38 ± 0.05$^{a}$ | 0.37 ± 0.05$^{a}$ | 0.37 ± 0.06 | 22 ± 8$^{b}$ | 18 ± 9$^{a}$ | 24 ± 7$^{b}$ | 17 ± 10 |
| Skull nearby De | 0.35 ± 0.07 | 0.35 ± 0.06 | 0.32 ± 0.06 | 0.32 ± 0.06 | 0.37 ± 0.06 | 12 ± 17 | −1 ± 16 | 0 ± 15 | 20 ± 16 |
| Skull remote | 0.43 ± 0.02 | 0.46 ± 0.03$^{a}$ | 0.50 ± 0.03$^{c}$ | 0.49 ± 0.03$^{c}$ | 0.46 ± 0.02$^{a}$ | 10 ± 5$^{a}$ | 20 ± 5$^{c}$ | 17 ± 4$^{c}$ | 10 ± 4$^{a}$ |

Values are presented as mean ± SE.
$^{a,b,c}$Differences from Pre: $^{a}P < 0.05$, $^{b}P < 0.01$, $^{c}P < 0.001$ (linear mixed model analysis with pairwise comparisons).

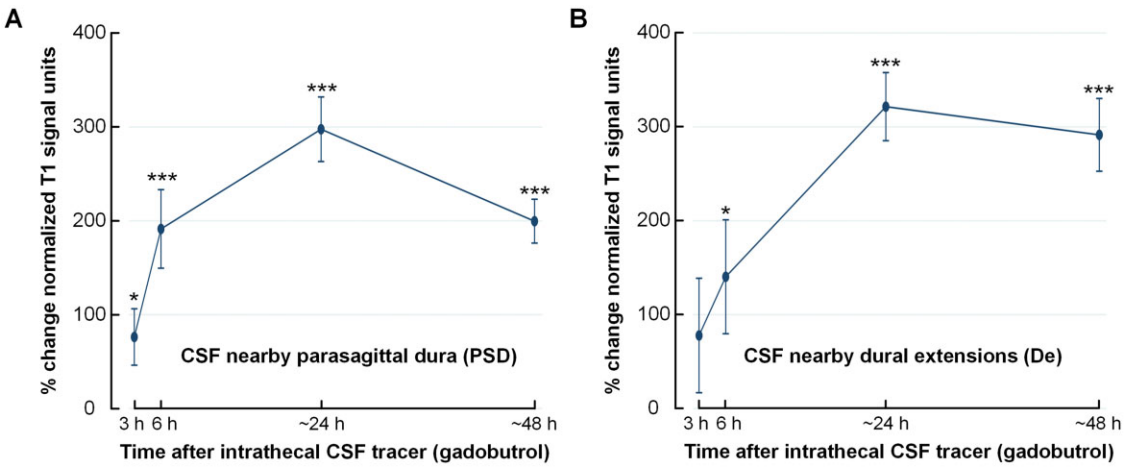


**Figure 3 Tracer enrichment over time in CSF of subarachnoid space nearby the regions of interest.** Tracer enrichment in CSF of subarachnoid space (**A**) nearby PSD ($n = 47$) and (**B**) and nearby De to diploe of skull bone in distance from PSD ($n = 12$). The percentage change in normalized $T_1$-BB signal, indicative of tracer enrichment, was highly significant in both locations (linear mixed model analysis; $^{*}P < 0.05$, $^{**}P < 0.01$, $^{***}P < 0.001$), with peak at 24 h. Trend plots presented by mean and error bars as standard errors.

changes in normalized $T_1$-BB signal over time, including percentage changes within the different dural locations enriched with tracer.

There was a highly significant correlation between the enrichment of tracer within PSDe and within CSF (Supplementary Fig. 10). Likewise, there was a highly significant correlation between tracer enrichment within De and within CSF (Supplementary Fig. 11).

## Tracer enrichment in skull bone marrow

Table 2 provides an overview of changes over time for normalized $T_1$-BB signal and percentage change within the different skull bone marrow locations enriched with tracer. The percentage change in normalized $T_1$-BB signal within skull bone marrow is further illustrated in Fig. 5. There was moderate, but highly significant tracer enrichment in skull bone marrow nearby PSD (Fig. 5A) and nearby PSDe (Fig. 5B). This was not significant nearby De, but there was extensive inter-individual variation and lower number of observations of De ($n = 12$; Fig. 5C). In skull bone marrow remote to PSD, PSDe and De, there was also a time-dependent change in tracer enrichment (Fig. 5D), providing evidence that tracer passes directly from CSF to skull bone marrow, independent of PSD, PSDe and De.

## Tracer enrichment in parasagittal dura and nearby skull bone marrow depends on the underlying brain disease

The present data further provide preliminary evidence that molecular transport to dural tissue and skull bone marrow may differ between brain diseases. Supplementary Table 1 presents differences between disease categories with different types of intracranial pathology, with regard to tracer enrichment. Tracer enrichment in PSD was found among all subgroups, while enrichment in nearby skull bone was detected in idiopathic normal pressure hydrocephalus, communicating hydrocephalus and idiopathic intracranial hypertension, while not in spontaneous intracranial hypotension, arachnoid cysts and reference subjects. In idiopathic intracranial hypertension, a neurological disease characterized by increased intracranial pressure as well as impaired glymphatic function,[19] tracer enrichment was significantly reduced in PSD at 24 and 48 h (Supplementary Fig. 12A), while enrichment in nearby skull bone marrow was unchanged (Supplementary Fig. 12B). In two

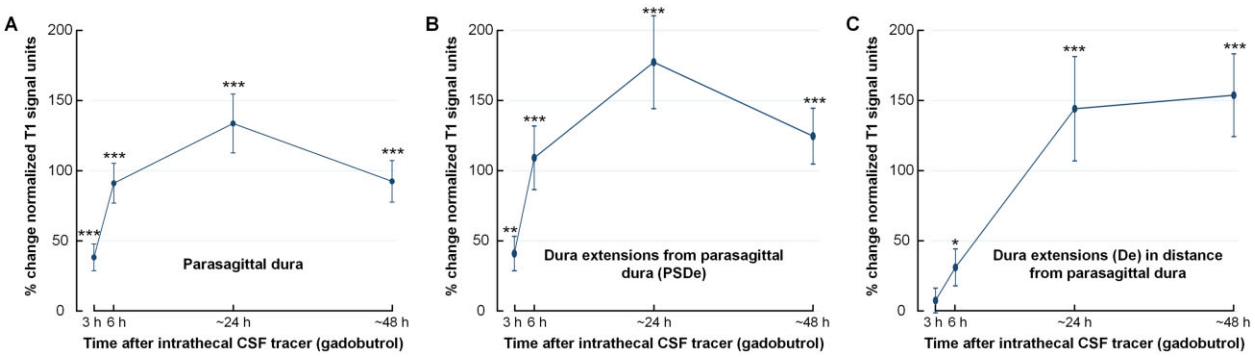


**Figure 4 Tracer enrichment in different intradural locations.** Tracer (gadobutrol) enrichment over time within (**A**) PSD ($n = 47$), (**B**) PSDe ($n = 27$) and (**C**) within De into diploe of skull bone marrow in distance from PSD ($n = 12$). The plots show tracer enrichment as a percentage change in normalized $T_1$-BB signal units. The signal change, indicative of tracer enrichment, was highly significant for all locations (linear mixed model analysis; $^{*}P < 0.05$, $^{**}P < 0.01$, $^{***}P < 0.001$), with peak at 24 h. Trend plots presented by mean and error bars as standard errors.

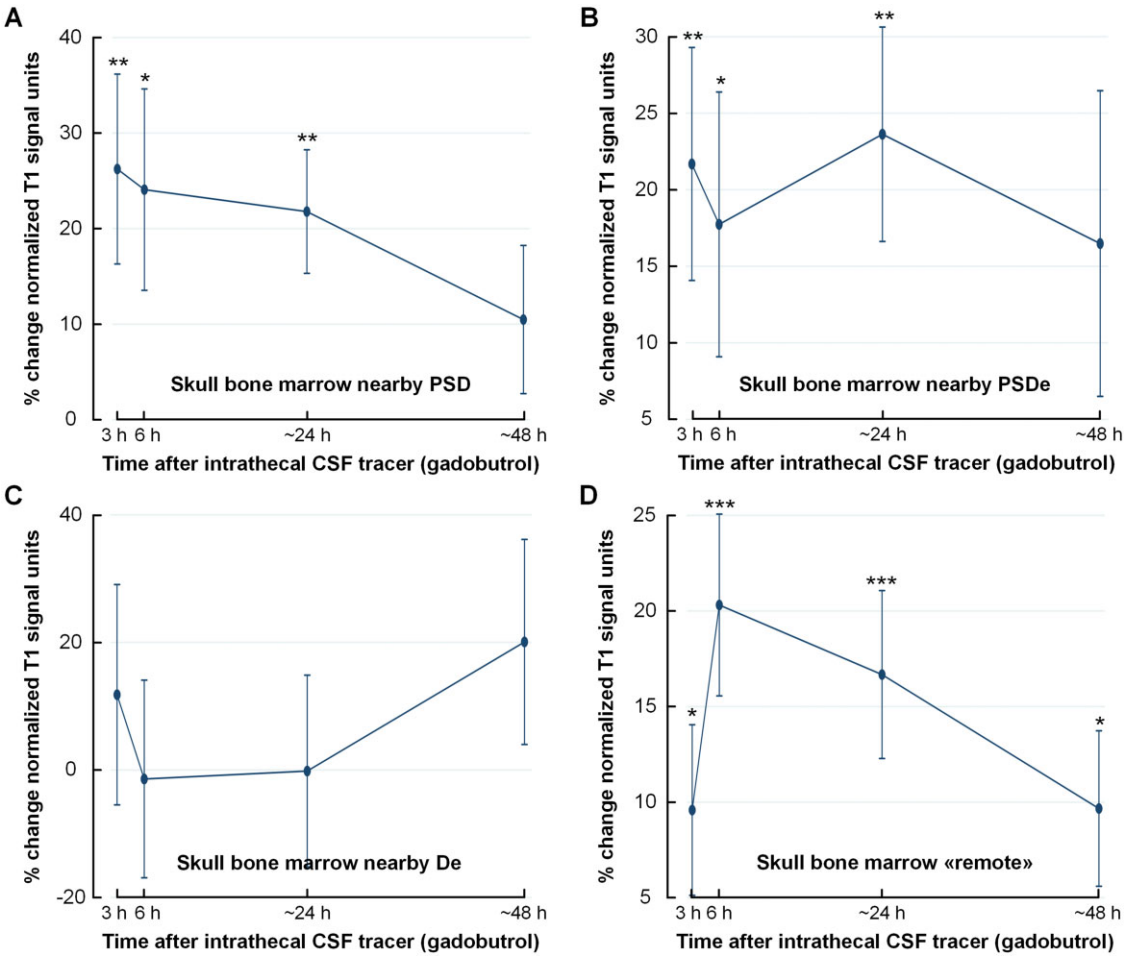


**Figure 5 Tracer enrichment within skull bone within different regions of interest.** Tracer (gadobutrol) enrichment over time in different regions of skull bone marrow. (**A**) Skull bone marrow nearby PSD ($n = 47$). (**B**) Skull bone marrow nearby dural extensions from parasagittal dura (PSDe) to diploe ($n = 27$). (**C**) Skull bone marrow nearby dural extensions (De) to diploe in distance from the PSD ($n = 12$). (**D**) Skull bone marrow in distance from visible intradural tracer enrichment, denoted 'remote' ($n = 47$). The plots show the percentage change in normalized $T_1$-BB signal units. The signal change, indicative of tracer enrichment, was highly significant for several locations (linear mixed model analysis; $^{*}P < 0.05$, $^{**}P < 0.01$, $^{***}P < 0.001$), with peak at 24 h. Trend plots presented by mean and error bars as standard errors.

individuals with so-called idiopathic normal pressure hydrocephalus, a subtype of dementia with close overlaps with Alzheimer's [20], tracer levels showed a different pattern than idiopathic intracranial hypertension, with significantly increased tracer level in skull bone marrow at 48 h (Supplementary Fig. 12C and D). Even though numbers are low, patients with evidence of CSF blockade due to cerebral cysts, showed another pattern in tracer enrichment in PSD than references (Supplementary Fig. 13A and B).

## Discussion

As a carrier of substances to and from the entire brain, CSF has emerged to play a crucial role in the pathogenesis behind inflammatory and degenerative brain diseases. Still, CSF efflux pathways from the subarachnoid compartment have remained incompletely understood, particularly in humans, where *in vivo* CSF tracer studies have been scarce. Here, we extend previous observations of trans-arachnoid efflux of tracer to the PSD,[5] and demonstrate CSF efflux also into the diploic space at the skull vertex in a patient cohort. The results indicate the existence of a pathway for direct communication between the brain and bone marrow, enabling for immune surveillance at the meninges exerted by constituents of the central immune system.

Entry of CSF tracer into dura demonstrates passage of a low-molecular weight compound across the human arachnoid barrier, even though the particular routes for this molecular egress remain obscure at 1-mm image resolution at MRI. In line with the traditional view, a CSF tracer study of mice found no signs of tracer propagation beyond the arachnoid layer.[21] On the other hand, it was recently microscopically visualized endothelial lined gaps and fissures in PSD of pigs, suggesting a local drainage pathway for CSF.[22] Another group demonstrated that a subset of arachnoid granulations in humans may drain CSF via lymphatic vessels to the venous circulation.[23] Furthermore, the adjacent dural sinus stroma was found to function as an immune hub allowing for CNS immune surveillance by trafficking T cells,[7] underlining the crucial role of this region for cross-talk between CNS-derived antigens and the peripheral immune system. However, the current findings of tracer enhancement in bone marrow at the skull vertex even remote to intradiploic dural extensions, indicate other physical connections between CSF and the bone marrow space in humans may also exist. This is corroborated by the findings of Roth *et al.*[9] who found the intact rodent skull bone permeable to small molecular weight compounds up to 40 000. Herrison *et al.*[11] demonstrated that neutrophils derived from murine skull bone marrow contributed in early cerebral inflammation via dura by direct connections through the inner skull cortex, connections that were also shown to be present in the outer skull cortex of human subjects. Accumulated evidences have demonstrated active function and trafficking of immune cells within bone marrow, including T cells.[24] In a rodent study, activated T cells were shown to participate in neuroinflammation subsequent to entry from the leptomeninges into CSF, where even remote areas of the CNS could be reached.[12] CSF is an effective carrier medium for wide cranio-spinal distribution of substances, primarily along the fluid spaces at the CNS surface, but also within the CNS itself. After intrathecal administration of gadobutrol at the lumbar level in human subjects, its brain-wide distribution could be confirmed after 24 h,[16] and was suggested to enter brain tissue in part along perivascular spaces as proposed in the glymphatic system[15] and by diffusion,[25] which may be a dominating factor for low-molecular weight substances.

A potential two-way communication between bone marrow and CSF may have broad implications for the clinical interpretation of common, but by large inadequately explained symptoms in conditions where bone marrow activation occurs, for instance in influenza virus illness[26] and SARS-CoV-2 (COVID-19).[27] Headache may in these conditions thus potentially be derived from inflammation of anatomical structures harbouring pain receptors, such as the meninges and skull bone marrow.[28] In sickness behaviour, which is strongly associated with pro-inflammatory cytokines reaching the CNS, the large size of these molecules has meant they have been considered unlikely to passively migrate through the BBB, and it has therefore remained equivocal how they exert their effect on the brain.[29] An alternative hypothesis may be that cytokines enter the brain directly via CSF from meninges and even adjacent bone marrow. The impact of meningeal immunity has furthermore been reported to influence memory function,[30] anxiety,[31] brain tumors[32,33] and neurodegenerative diseases such as Parkinson's[34] and Alzheimer's disease.[35] For example, neuro-inflammation may have a critical role in neurodegeneration, as illustrated by the findings of an adaptive immune response in CSF in Alzheimer's disease, and antigen-experienced T cells patrolling the intrathecal space in age-related neurodegeneration.[36]

With regard to CSF clearance of neurotoxic solutes involved in neurodegeneration, human data suggest CSF resorption capacity at the upper brain convexities plays a minor role, as tracer clearance from CSF peaks in blood far earlier than peak levels are reached in CSF underneath the skull vertex.[37] The relative importance of meningeal lymphatic vessels for egress of neurotoxic metabolites in neurodegenerative disease needs to be further studied. Experimental data have shown that impaired meningeal lymphatic function caused reduced paravascular influx of macromolecules into the brain, and reduced efflux from the interstitial space.[35] We previously reported that peak CSF tracer enhancement in human brain and cervical lymph nodes concurred in time.[38]

In the present study, we tracked *in vivo* molecular efflux from CSF to dura and skull vertex after intrathecal administration of the macrocyclic MRI contrast agent gadobutrol. Even though this is off-label use, the safety of intrathecal gadobutrol in doses of 0.5 mmol and less has been documented in previous studies.[39–41] Gadobutrol is sensitively detected at $T_1$-weighted MRI and well suited as a CSF tracer by being an exogenous, highly hydrophilic compound and further characterized by its stability and inertia. After intrathecal administration, the molecule is contained outside the intact blood–brain barrier, thereby preventing leakage into healthy brain vessels and thus traces solely the extra-vascular CSF pathways. It should be noted that the small molecular size (molecular weight 604 Da) and hydrophilic properties renders gadobutrol susceptible to diffusional properties in tissue.[25] The detection of CSF tracer in bone marrow adjacent to dural tissue could therefore be expected to represent diffusion from dura to bone marrow along a concentration gradient, also suggested by the finding of far less percentage tracer enrichment in bone marrow than the adjacent dural structures at any time point. Gadobutrol might also pass along small diploic veins from dura to diploe, given previous observations in humans of small channels at the inner skull wherein diploic veins of diameter about 1.5 mm reside.[11] Furthermore, the tracer molecule may have been resorbed to an unknown extent by dural lymphatic and dural blood vessels, which lack tight junctions, thus allowing for leakage of gadobutrol directly into blood. This may also be a reason why there was no significant increase in skull bone marrow adjacent to the more laterally located dural intradiploic extensions.

We used FLAIR-imaging to identify areas of dural soft tissue extending into the diploic skull space, both in parasagittal and more lateral locations discontinuous with the PSD, all typically situated near the vertex of the cranial vault. Within these, CSF tracer enhancement was assessed by using $T_1$-weighted images with the BB technique, which incorporates suppression of voxel elements in motion. Measurements were performed only in tissue deemed stationary from the combined findings at FLAIR- and $T_1$ BB MRI. To this end, we excluded diploic veins from measurements, which are susceptible to signal loss from flowing effects, even if not obviously suppressed at $T_1$ BB. However, we note that diploic veins often run in direct continuity with intradiploic dural extensions (Figs 1 and 2). In a previous work,[42] diploic meningeal extensions were coined cranial arachnoid protrusions and suggested to drain

CSF further into contiguous diploic veins belonging to an extensive network throughout the cranium. In contrast to this previous study using $T_2$- and contrast enhanced $T_1$-weighted imaging for assessment, we used FLAIR- and $T_1$ BB MRI to separate meningeal structures from CSF (low signal at FLAIR) and blood flow (low signal at $T_1$ BB). Using this approach, we note that the stromal, soft tissue-like nature of the meningeal extensions into dura resemble primarily the dura, and therefore consistently use the term (parasagittal) dural extension.

The cranial bone marrow is previously reported to be heterogeneous, with the diploe becoming gradually thicker and containing more yellow marrow with age,[43] with the most obvious change at MRI occurring typically from first years of life to young adulthood. In this study, the mean age of participants was 43 years and individuals below 18 years of age were not included. However, inter-individual and regional differences in diploic thickness also occur within same age groups, and in some subjects the diploic space remains thin, at least in some regions. We therefore manually adjusted region of interest size to the thickness of diploe, aiming to restrict the region of interest borders well within inner and outer borders of cortical bone, but still as close to intradiploic dural extensions as possible to maximize sensitivity for tracer detection in bone marrow. Our voxel size of 1 $mm^3$ should in this regard be considered reasonable to minimize any influence of local partial averaging effects from surrounding non-marrow tissue elements. It should also be noted that due to the resolution of MRI ($1 \times 1 \times 1\,mm^3$), it is not possible to visualize meningeal lymphatic vessels of submillimetre cross-sectional diameter.[2,3,44] Moreover, the tracer enrichment does not compare with the arachnoid granulations within the dural sinuses.[45]

Some limitations should be noted. Change in $T_1$-BB signal was assessed by manually placing regions of interest. While care was taken to avoid compact cortical bone and thereby partial volume effects, this may have introduced some uncertainty. Moreover, some uncertainty may have been introduced by changes in MRI grey scale between MRI acquisitions even though we assessed normalized $T_1$-BB signal units. These normalized values provide a semi-quantitative determination of tracer level. Exact quantitative measures are, however, out of scope at this moment.

Another limitation is that the study included symptomatic patients and the observations are necessarily not transferable to healthy asymptomatic subjects. No CSF disorder was diagnosed in 15/53, and reference subjects may therefore be considered close to healthy. In these, no enrichment of CSF tracer could be detected in bone marrow (Supplementary Table 1). Each of the other patient categories included few subjects, but the finding of significant bone marrow tracer enrichment in idiopathic normal pressure hydrocephalus, communicating hydrocephalus and idiopathic intracranial hypertension subgroups, may suggest that molecular interchange between CSF and bone marrow is more associated with CSF disorders than normal physiology. This would be an important research question in future studies.

Finally, we cannot completely exclude that the signal increase in bone marrow may be derived from circulating gadobutrol in blood. Following a standard intravenous dose of MRI contrast agent, signal intensity may indeed increase 3–59% with the maximum increase within the first 15 min, typically more in younger than older subjects.[46] At a standard intravenous dose of 0.1 mmol gadobutrol/kg body weight (typically 8 ml in a 80-kg patient), an average of 0.59 mmol gadobutrol/l plasma has been measured 2 min after the injection and 0.3 mmol gadobutrol/l plasma 60 min postinjection (https://www.medicines.org.uk/emc/product/2876/smpc#gref). After intrathecal injection of a total amount of 0.5 mmol (~6% of the typical intravenous dose), we obtained blood samples in parallel with MRI scans and measured plasma concentrations at the order ~0.5–2.0 μmol,[37] i.e. about 1/1000 the amount in plasma compared to after the intravenous administration. It is therefore highly unlikely that our observed signal increase in skull bone marrow should be derived from contrast agent circulating in the blood.

In conclusion, this study demonstrates *in vivo* molecular efflux from CSF to dura, to extensions of dura into skull bone marrow, and to bone marrow itself in patients with CSF circulation disorders. The lack of impermeable barriers between CSF and the intradiploic skull space suggests that human bone marrow derived solutes and cells may participate in CNS immune surveillance at the meninges, and also be carried by CSF directly into CNS.

## Acknowledgements

The authors thank Dr Øivind Gjertsen, Dr Bård Nedregaard and Dr Ruth Sletteberg from the Department of Radiology, Oslo University Hospital—Rikshospitalet, who performed the intrathecal gadobutrol injections in all study subjects. We also sincerely thank the Intervention Centre and Department of neurosurgery at Oslo University Hospital-Rikshospitalet for providing valuable support with MR scanning and care-taking of all study subjects throughout the study. The authors thank Are Hugo Pripp, PhD, Department of Biostatistics, Epidemiology and Health Economics, Oslo University Hospital, Oslo, for statistical help during preparation of the paper.

## Funding

Department of Neurosurgery, Oslo University Hospital—Rikshospitalet, Oslo, Norway.

## Competing interests

G.R. received a fee for speaking at the Bayer symposium at the European Congress of Radiology 2020 (Vienna, Austria). The authors declare no other conflict of interests.

## Supplementary material

Supplementary material is available at *Brain* online.

## References

1. Abbott NJ. Evidence for bulk flow of brain interstitial fluid: Significance for physiology and pathology. *Neurochem Int*. 2004; 45(4):545–552.
2. Louveau A, Smirnov I, Keyes TJ, et al. Structural and functional features of central nervous system lymphatic vessels. *Nature*. 2015;523(7560):337–341.
3. Aspelund A, Antila S, Proulx ST, et al. A dural lymphatic vascular system that drains brain interstitial fluid and macromolecules. *J Exp Med*. 2015;212(7):991–999.
4. Jacob L, Boisserand LSB, Geraldo LHM, et al. Anatomy and function of the vertebral column lymphatic network in mice. *Nat Commun*. 2019;10(1):4594.
5. Ringstad G, Eide PK. Cerebrospinal fluid tracer efflux to parasagittal dura in humans. *Nat Commun*. 2020;11(1):354.
6. Mastorakos P, McGavern D. The anatomy and immunology of vasculature in the central nervous system. *Sci Immunol*. 2019; 4(37):eaav0492.
7. Rustenhoven J, Drieu A, Mamuladze T, et al. Functional characterization of the dural sinuses as a neuroimmune interface. *Cell*. 2021;184(4):1000–1016.e27.

8. Cugurra A, Mamuladze T, Rustenhoven J, et al. Skull and vertebral bone marrow are myeloid cell reservoirs for the meninges and CNS parenchyma. *Science*. 2021;373(6553):eabf7844.
9. Roth TL, Nayak D, Atanasijevic T, Koretsky AP, Latour LL, McGavern DB. Transcranial amelioration of inflammation and cell death after brain injury. *Nature*. 2014;505(7482):223–228.
10. Li Y, Wang W, Yang F, Xu Y, Feng C, Zhao Y. The regulatory roles of neutrophils in adaptive immunity. *Cell Commun Signal*. 2019; 17(1):147.
11. Herisson F, Frodermann V, Courties G, et al. Direct vascular channels connect skull bone marrow and the brain surface enabling myeloid cell migration. *Nat Neurosci*. 2018;21(9):1209–1217.
12. Schläger C, Körner H, Krueger M, et al. Effector T-cell trafficking between the leptomeninges and the cerebrospinal fluid. *Nature*. 2016;530(7590):349–353.
13. Castro Dias M, Mapunda JA, Vladymyrov M, Engelhardt B. Structure and junctional complexes of endothelial, epithelial and glial brain barriers. *Int J Mol Sci*. 2019;20(21):5372.
14. Hadjikhani N, Albrecht DS, Mainero C, et al. Extra-axial inflammatory signal in parameninges in migraine with visual aura. *Ann Neurol*. 2020;87(6):939–949.
15. Iliff JJ, Wang M, Liao Y, et al. A paravascular pathway facilitates CSF flow through the brain parenchyma and the clearance of interstitial solutes, including amyloid beta. *Sci Transl Med*. 2012; 4(147):147ra111.
16. Ringstad G, Valnes LM, Dale AM, et al. Brain-wide glymphatic enhancement and clearance in humans assessed with MRI. *JCI Insight*. 2018;3(13):1–16.
17. Bakshi R, Ariyaratana S, Benedict RH, Jacobs L. Fluid-attenuated inversion recovery magnetic resonance imaging detects cortical and juxtacortical multiple sclerosis lesions. *Arch Neurol*. 2001; 58(5):742–748.
18. Mandell DM, Mossa-Basha M, Qiao Y, et al.; Vessel Wall Imaging Study Group of the American Society of Neuroradiology. Intracranial vessel wall MRI: Principles and expert consensus recommendations of the American society of neuroradiology. *AJNR Am J Neuroradiol*. 2017;38(2):218–229.
19. Eide PK, Pripp AH, Ringstad G, Valnes LM. Impaired glymphatic function in idiopathic intracranial hypertension. *Brain Commun*. 2021;3(2):fcab043.
20. Leinonen V, Koivisto AM, Savolainen S, et al. Amyloid and tau proteins in cortical brain biopsy and Alzheimer's disease. *Ann Neurol*. 2010;68(4):446–453.
21. Ma Q, Ineichen BV, Detmar M, Proulx ST. Outflow of cerebrospinal fluid is predominantly through lymphatic vessels and is reduced in aged mice. *Nat Commun*. 2017;8(1):1434.
22. Kutomi O, Takeda S. Identification of lymphatic endothelium in cranial arachnoid granulation-like dural gap. *Microscopy (Oxf)*. 2020;69(6):391–400.
23. Yağmurlu K, Sokolowski J, Soldozy S, et al. A subset of arachnoid granulations in humans drain to the venous circulation via intradural lymphatic vascular channels. *J Neurosurg*. 2021; 1-10. https://doi.org/10.3171/2021.2.Jns204455.
24. Zhao E, Xu H, Wang L, et al. Bone marrow and the control of immunity. *Cell Mol Immunol*. 2012;9(1):11–19.
25. Valnes LM, Mitusch SK, Ringstad G, Eide PK, Funke SW, Mardal KA. Apparent diffusion coefficient estimates based on 24 hours tracer movement support glymphatic transport in human cerebral cortex. *Sci Rep*. 2020;10(1):9176.
26. Khatri M, Saif YM. Influenza virus infects bone marrow mesenchymal stromal cells in vitro: Implications for bone marrow transplantation. *Cell Transplant*. 2013;22(3):461–468.
27. Harris CK, Hung YP, Nielsen GP, Stone JR, Ferry JA. Bone marrow and peripheral blood findings in patients infected by SARS-CoV-2. *Am J Clin Pathol*. 2021;155(5):627–637.
28. Kosaras B, Jakubowski M, Kainz V, Burstein R. Sensory innervation of the calvarial bones of the mouse. *J Comp Neurol*. 2009; 515(3):331–348.
29. Shattuck EC, Muehlenbein MP. Human sickness behavior: Ultimate and proximate explanations. *Am J Phys Anthropol*. 2015;157(1):1–18.
30. Derecki NC, Cardani AN, Yang CH, et al. Regulation of learning and memory by meningeal immunity: A key role for IL-4. *J Exp Med*. 2010;207(5):1067–1080.
31. Alves de Lima K, Rustenhoven J, Da Mesquita S, et al. Meningeal γδ T cells regulate anxiety-like behavior via IL-17a signaling in neurons. *Nat Immunol*. 2020;21(11):1421–1429.
32. Hu X, Deng Q, Ma L, et al. Meningeal lymphatic vessels regulate brain tumor drainage and immunity. *Cell Res*. 2020;30(3): 229–243.
33. Song E, Mao T, Dong H, et al. VEGF-C-driven lymphatic drainage enables immunosurveillance of brain tumours. *Nature*. 2020; 577(7792):689–694.
34. Ding XB, Wang XX, Xia DH, et al. Impaired meningeal lymphatic drainage in patients with idiopathic Parkinson's disease. *Nat Med*. 2021;27(3):411–418.
35. Da Mesquita S, Louveau A, Vaccari A, et al. Functional aspects of meningeal lymphatics in ageing and Alzheimer's disease. *Nature*. 2018;560(7717):185–191.
36. Gate D, Saligrama N, Leventhal O, et al. Clonally expanded CD8 T cells patrol the cerebrospinal fluid in Alzheimer's disease. *Nature*. 2020;577(7790):399–404.
37. Eide PK, Mariussen E, Uggerud H, et al. Clinical application of intrathecal gadobutrol for assessment of cerebrospinal fluid tracer clearance to blood. *JCI Insight*. 2021;6(9):e147063.
38. Eide PK, Vatnehol SAS, Emblem KE, Ringstad G. Magnetic resonance imaging provides evidence of glymphatic drainage from human brain to cervical lymph nodes. *Sci Rep*. 2018;8(1):7194.
39. Edeklev CS, Halvorsen M, Lovland G, et al. Intrathecal use of gadobutrol for glymphatic MR imaging: Prospective safety study of 100 patients. *AJNR Am J Neuroradiol*. 2019;40(8):1257–1264.
40. Halvorsen M, Edeklev CS, Fraser-Green J, et al. Off-label intrathecal use of gadobutrol: Safety study and comparison of administration protocols. *Neuroradiology*. 2021;63(1):51–61.
41. Patel M, Atyani A, Salameh JP, McInnes M, Chakraborty S. Safety of intrathecal administration of gadolinium-based contrast agents: A systematic review and meta-analysis. *Radiology*. 2020; 297(1):75–83.
42. Tsutsumi S, Ogino I, Miyajima M, et al. Cranial arachnoid protrusions and contiguous diploic veins in CSF drainage. *AJNR Am J Neuroradiol*. 2014;35(9):1735–1739.
43. Li Q, Pan SN, Yin YM, et al. Normal cranial bone marrow MR imaging pattern with age-related ADC value distribution. *Eur J Radiol*. 2011;80(2):471–477.
44. Absinta M, Ha SK, Nair G, et al. Human and nonhuman primate meninges harbor lymphatic vessels that can be visualized noninvasively by MRI. *Elife*. 2017;6:e29738.
45. Trimble CR, Harnsberger HR, Castillo M, Brant-Zawadzki M, Osborn AG. 'Giant' arachnoid granulations just like CSF?: NOT!! *AJNR Am J Neuroradiol*. 2010;31(9):1724–1728.
46. Baur A, Stäbler A, Bartl R, Lamerz R, Scheidler J, Reiser M. MRI gadolinium enhancement of bone marrow: Age-related changes in normals and in diffuse neoplastic infiltration. *Skeletal Radiol*. 1997;26(7):414–418.